Bulletin of the Seismological Society of America, Vol. 98, No. 2, pp. 797–803, April 2008, doi: 10.1785/0120060238

Ⓔ

Short Note

High-Frequency Shear-Wave Propagation across the Hellenic Subduction Zone

by K. I. Konstantinou and N. S. Melis

Abstract This study investigates shear-wave propagation across the Hellenic subduction zone using high-quality waveforms of 71 intermediate-depth events (40–160-km depth). The data have been recorded by a permanent seismic network consisting of 22 broadband, three-component stations that cover most parts of Greece. Shear waves can be efficiently transmitted with low attenuation ($Q_s \sim 1100$) through the descending slab, which extends laterally over much of the forearc area with a northwest–southeast strike. The slab also appears to be continuous downdip in the depth range 60–160 km, even though it was found that a gap smaller than 10 km would not affect shear-wave efficiency significantly. Two highly attenuating areas have been detected, one in the central/southeast Aegean corresponding to the mantle wedge and the other in the northern Aegean, probably caused by elevated upper mantle temperatures owing to the ongoing extension in that area. These results provide additional constraints for the geometry of the Hellenic subduction zone and the geodynamic setting of the Aegean region.

Online Material: *S*-wave ray paths, *P*-velocity model, and source parameters of selected events.

Introduction

The efficiency of shear-wave propagation across subduction zones is considered as a sensitive indicator of the upper-mantle 3D structure and rheology (e.g., Mele, 1998). This can be explained based on the observation that shear waves are strongly attenuated as they travel through partially molten regions of the mantle, such as the mantle wedge, while they propagate efficiently within the cold, high-strength lithospheric slab. Such propagation characteristics have been used in the past to further constrain the geometry of subduction zones (Oliver and Isacks, 1967; Barazangi and Isacks, 1971; Barazangi *et al.*, 1972; Barazangi *et al.*, 1973; Mele, 1998). More recently, numerous studies have successfully inverted attenuation parameters of earthquakes occurring in subduction zones in order to derive the 3D attenuation structure of the slab and mantle wedge (e.g., Roth *et al.*, 1999; Tsumura *et al.*, 2000; Eberhart-Phillips and Chadwick, 2002; Salah and Zhao, 2003; Schurr *et al.*, 2003; Stachnik *et al.*, 2004). These studies have confirmed quantitatively that anelastic attenuation is particularly high inside the mantle wedge ($Q_s \sim 45$–283), while it is considerably lower ($Q_s \geqq 1000$) within the subducting slab.

The tectonic setting of the south Aegean Sea is characterized by the northward movement of the African plate relative to Eurasia at a rate of 1 cm/yr (DeMets *et al.*, 1990) and its subduction along the Hellenic arc (Fig. 1). This process is responsible for the formation of active volcanic centers and a well-defined Wadati–Benioff zone extending down to a depth of 180 km, as confirmed from the distribution of earthquake hypocenters (Papazachos *et al.*, 2000). Large-scale features of the subducting slab in terms of thickness and dip have been identified up to a depth of 600 km using teleseismic travel-time tomography (Spakman *et al.*, 1988). Finer details of the shallow part of the slab (<150 km), such as a prominent kink at a depth of 70 km, have been highlighted after inverting travel times of regional earthquakes (Papazachos and Nolet, 1997). However, the relatively limited resolution of these tomographic images, especially in the eastern part of the subduction zone, has left several unresolved issues concerning the geometry of the subduction.

Delibasis (1982) was the first to systematically investigate the efficiency of shear-wave propagation across the Hellenic subduction zone. He observed a pronounced attenuation for ray paths that traversed central Aegean Sea, presumably due to the effect of the mantle wedge. The limited number of available stations as well as the poor

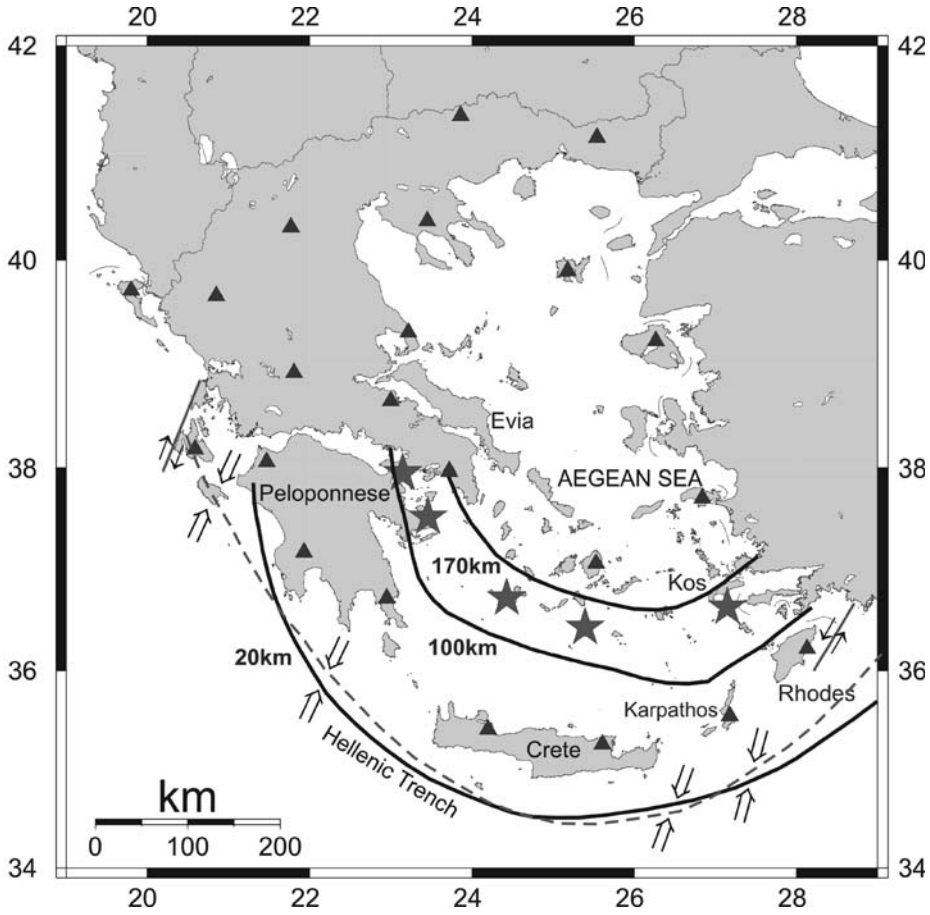

Figure 1. Map showing the tectonic setting of the broader Aegean Sea region and the isodepth curves for earthquake foci at 20, 100, and 170 km after Papazachos *et al.* (2000). The Hellenic Trench is noted with a dashed line, and the arrows indicate the sense of the compressive stress field along the subduction (after Karagianni *et al.*, 2005). The two transform faults confine the two edges. Active volcanoes, stars; broadband seismic stations of the HL network, triangles.

data quality (short-period seismograms recorded on paper) hampered the accurate delineation of either the high attenuation area, or that of the subducting slab. On the other hand, Gök *et al.* (2000) used digital and analog waveform data from 32 stations in order to check *Sn*-wave propagation for an area stretching from western Greece to the Caucasus (longitude 20°–44°). The authors observed inefficient propagation for ray paths along the Aegean Sea and efficient propagation in western Greece.

This work studies the propagation characteristics of high-frequency shear waves across the Hellenic subduction zone, utilizing high-quality waveforms recorded by a permanent regional network. We use the efficiency of shear-wave propagation in order to map the lateral extent and downdip continuity of the high-strength slab and also to delineate the areas where significant shear-wave attenuation is observed. First, we give an overview of the available waveform data and describe the methodology used for characterizing each shear-wave ray path. Subsequently, we present the observations and discuss their implications in connection with the geodynamic properties of the Aegean Sea region.

Data and Methodology

The National Observatory of Athens Institute of Geodynamics operates the Hellenic (HL) Seismic Network (http://bbnet.gein.noa.gr, last accessed July 2008) that presently consists of 22 three-component, broadband (up to 20–30-sec) seismic stations recording continuous waveform data that are utilized for the seismic monitoring of the broader Greek region (Fig. 1). A detailed description of the network operation and routine data processing can be found in Melis and Konstantinou (2006). For the purpose of our study, we first compiled a list of all intermediate-depth events that occurred along the Hellenic subduction zone in the period 2000–2006 when high-quality digital data are available. The *P* and *S* phases of these events were manually picked, and the arrival times were inverted using Hypoinverse 2000 (HYPO2000) (Klein, 2002). We used a 1D velocity model that stems from the results of the tomographic study of Papazachos and Nolet (1997) (Ⓔ see Table S1 in the electronic edition of *BSSA*) and a V_P/V_S ratio of 1.78. The final selection of the events that are included here was based on the following criteria: (1) a signal-to-noise ratio of at least three for

most stations that recorded each particular event, (2) formal horizontal location errors that did not exceed 10 km, and (3) convergence of the location inversion to the same hypocentral depth even when different initial values were tried. Ⓔ Table S2 in the electronic edition of *BSSA* contains the locations and local magnitudes of the 71 selected earthquakes.

The methodology first proposed by Oliver and Isacks (1967) and later used by Mele (1998) and Gök *et al.* (2000) is applied for the classification of our waveform data. It is based on a qualitative analysis of waveforms, where the shear phase is classified in terms of propagation efficiency after considering its amplitude and frequency content relative to the compressional phase. Before characterizing the efficiency of observed *S* phases at any station, we high-pass filtered at 2 Hz the waveforms using a two-pole Butterworth filter and checked the resulting traces. This was done in order to eliminate any low-frequency noise and also to be able to compare the filtered and unfiltered shear phases for each trace. The horizontal components were later rotated into radial and transverse with respect to the epicenter of each event, and the waveforms were reviewed once more. In all of the cases, we found that rotation affected very little the appearance of the *S* phases and their characterization.

Following this procedure, we were able to discern three distinct groups of waveforms: (1) those exhibiting a high-frequency (>2 Hz), high-amplitude shear phase that was recorded by both horizontal components, (2) those exhibiting lack of a clear shear phase in one or both horizontal components, and (3) those exhibiting a shear phase composed of low-frequency ($\sim$1 Hz), low-amplitude waves. Ray paths corresponding to group (1) waveforms were characterized as efficient and those corresponding to group (2) or (3) as inefficient. Figure 2 shows typical examples of the waveform groups described here and their ray paths, respectively. In this way, we have characterized 709 source-to-receiver paths as efficient and 161 as inefficient, yielding a total of 870 ray paths.

This kind of ray path characterization implicitly assumes that the major factor controlling the appearance of waveforms is the propagation path. Other factors could also be source radiation effects or peculiar instrument/site response. The faulting style of intermediate-depth seismicity along the Hellenic arc includes different fault types and orientations (see Benetatos *et al.*, 2004) that precludes a systematic bias of our results. Peculiar instrument/site response can also be ruled out on the grounds that stations that record waveforms belonging to group (1) from one back azimuth, may record waveforms belonging to group (2) from another back azimuth and vice versa.

Observations

Shear waves can be efficiently transmitted across a subduction zone through the high-strength descending slab, which effectively forms a wave guide. Such a ray path would first travel upwards along the slab and then propagate to the station as an uppermost mantle *S* phase (Oliver and Isacks, 1967). The 709 efficient shear-wave ray paths included in this study are shown in Figure 3a. It can be seen that they cover the whole of the forearc area like the Peloponnese, Crete, Karpathos, and Rhodes islands and parts of northern/western Greece. A number of efficient rays also traverses the Turkish coast in a north-northwest–south-southeast direction. At this point, it should be noted that we did not observe for any of the studied events lack of shear phases at stations located in the forearc area. This implies efficient transmission of shear waves along the slab from all focal depths available in our dataset (40–160 km).

Inefficient transmission of shear waves can occur when traveling through anomalously hot mantle material. Figure 3b shows the 161 ray paths resulting from our analysis that exhibit this kind of behavior. It can be seen that stations in northern Greece as well as those in the north and east Aegean Sea do not record any shear waves, or the recorded waves are severely attenuated. The spatial pattern of inefficient propagation observed here also coincides with areas that usually report low-intensity values (II or less) during large intermediate-depth earthquakes (for a recent example, see Konstantinou *et al.*, 2006). A geographical sketch shown in Figure 4 summarizes the shear-wave propagation characteristics that we have observed.

Some of the events we have used in this study are located at more than 70-km depth; therefore, their ray paths may not be straight lines, as shown in Figure 3. In order to check whether the attenuation pattern we obtained is in any way biased by the focal depth, we plotted separately ray paths corresponding to events shallower than 70 km and those deeper than that (Ⓔ see Figure S1 in the electronic edition of *BSSA*). For efficient ray paths, the only difference we can observe is the increase in the number of rays corresponding to shallower events that traverse the western coast of Turkey. On the other hand, we find little difference between shallow and deeper events for inefficient ray paths. This leads us to the conclusion that focal depth is not the primary factor that is shaping the observed attenuation pattern.

Interpretation and Discussion

The surface expression of the propagation pattern of efficient shear-wave transmission can be related to the lateral extent of the subducted slab. The western part of the delineated slab is much larger than the eastern section in accordance with the tomographic model of Papazachos and Nolet (1997). This is probably due to the angle that the slab is dipping in the upper mantle and indicates that a steeper angle is needed for the eastern part as compared to the western one. Dipping angles calculated from the distribution of earthquake foci on the Wadati–Benioff zone agree with our observations and are in the range of 30° ($\pm$10°) for the western and 45° ($\pm$10°) for the eastern part (Papazachos *et al.*, 2000). The lateral extent boundary of the subducted slab has a

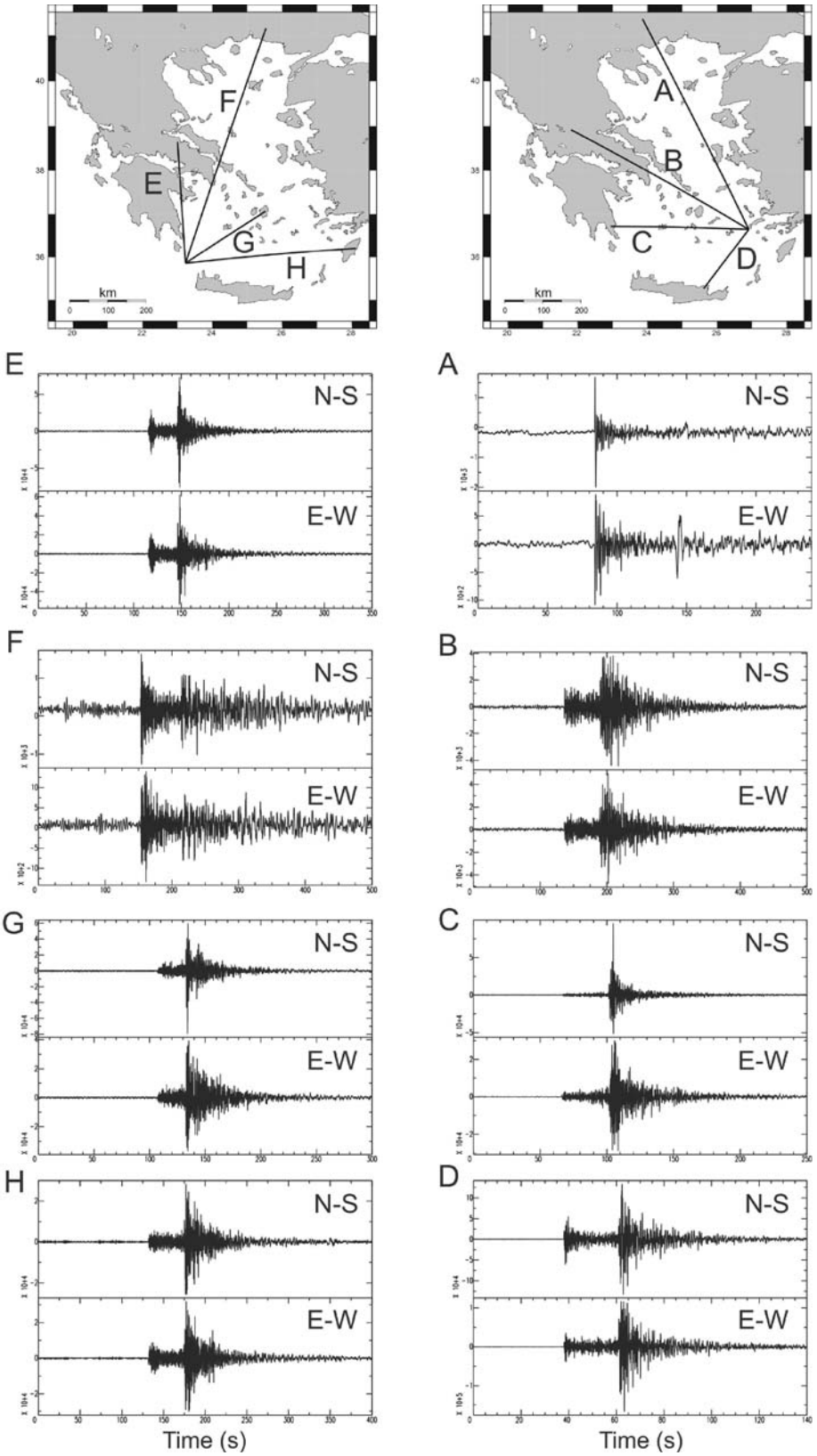

Figure 2. Examples of source-to-receiver ray paths (Ⓔ events 13 September 2003 and 4 November 2004 in Table S2 in the electronic edition of *BSSA*) and corresponding recorded velocity waveforms (amplitudes are in counts) for inefficient shear-wave transmission (a) and (f) and efficient shear-wave transmission (b), (c), (d), (e), (g), and (h).

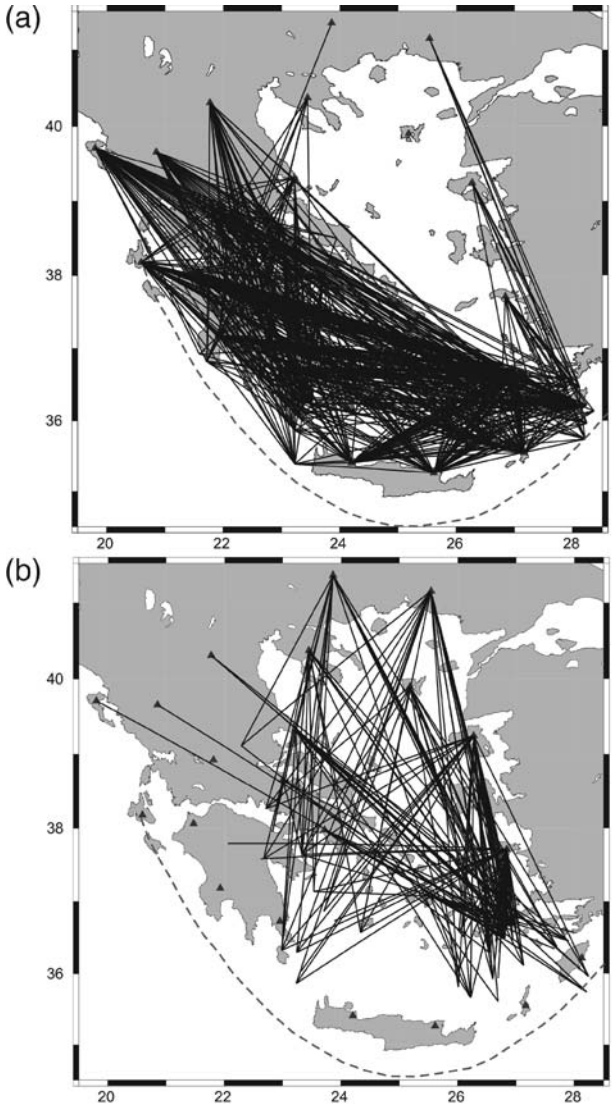

Figure 3. Maps showing (a) the 709 efficient shear-wave ray paths and (b) the 161 inefficient shear-wave ray paths, respectively. Other symbols same as in Figure 1.

northwest–southeast direction, traversing close to Evia island and the central Aegean before terminating near the western tip of Kos island. This boundary does not appear to be an artifact because it is defined by a large number of ray paths, while source location errors are too small (< 10 km) to introduce any substantial shifting to the direction of the rays. Its observed strike is also consistent with the resistivity mapping of the slab using magnetotelluric data (Galanopoulos *et al.*, 2005) and the modeling of regional gravity data (Tsokas and Hansen, 1997).

The downdip continuity of the descending slab has been questioned by Papazachos *et al.* (2000), who observed a gap in the distribution of earthquake foci occurring along the Wadati–Benioff zone at depths 80–100 km. As mentioned earlier, we observed efficient shear-wave phases at all the forearc stations available, which in turn suggests that the slab is continuous downdip for the earthquake depths considered in this study. However, as pointed out by Mele (1998), if a small gap exists along the dip of the slab, the efficiency of shear waves would not be significantly affected. Our waveform data can be used in order to investigate this point further by estimating the value of Q_s for different depths along the slab. Assuming that two earthquakes of similar magnitude but different focal depth are aligned to a station that records efficient shear waves, then their spectral ratio will be given by (Mele, 1998)

$$R(f) = A_{M1}(f)/A_{M2}(f) = [S_{M1}(f)/S_{M2}(f)](R_1/R_2)e^{-\pi(R_1-R_2)f/V_sQ_s}$$

where $A_{M1}(f)$ and $A_{M2}(f)$ are spectra of shear waves recorded at the same station from events 1 and 2, R_1 and R_2 are the distances from the hypocenter to the station, V_s is the shear-wave velocity, while $S_{M1}(f)$ and $S_{M2}(f)$ are the source spectra. The logarithm of the spectral ratio $R(f)$ is expected to be a linear function of frequency, whose slope is controlled by the value of $1/Q_s$.

We calculated such spectral ratios for earthquake pairs at five different depth ranges (60–75, 95–140, 95–155, 100–140, and 130–160 km). First, a cosine-tapered window of the shear phase for each of the two earthquakes considered was taken and fast Fourier transform was used in order to obtain their amplitude spectra. Spectral division yielded the ratio variation as a function of frequency for each pair as shown in Figure 5. The spectral ratio decay observed is consistent with an average $Q_s \sim 1100$ that is in agreement with Q values obtained for the forearc Aegean region by Hashida *et al.* (1988) from the inversion of seismic intensity data and Q_s values for the slab measured in other subduction zones like Japan (e.g., Umino and Hasegawa, 1984). The expected decay for paths that include a hypothetical gap of length 10 and 20 km is shown in Figure 5 by the two straight lines, respectively, assuming $Q_s \sim 50$ inside asthenospheric materials, and V_s is 4.4 km/sec. As the line representing the decay for the path that includes a gap of 10 km is more consistent with the data, we conclude that this is the smallest gap that can be resolved by our analysis.

Paths exhibiting inefficient transmission of shear waves can be divided into two separate groups based on back azimuth: ray paths of events that originate in the southern or southeastern Aegean and those of events originating in the Pelloponnese/central Greece. The inefficiency of the first group of ray paths can be explained by their passage through the partially molten mantle wedge. In a recent study, Karagianni *et al.* (2005) delineated an area of low shear-wave velocities (3.6–3.8 km/sec) below the Moho in central/southeastern Aegean (see geographical sketch in Fig. 4) that was interpreted as the manifestation of slab dehydration fluids/partial melt. Most of the inefficient ray paths belonging to the first group are passing through this area, which was also roughly highlighted by Delibasis (1982).

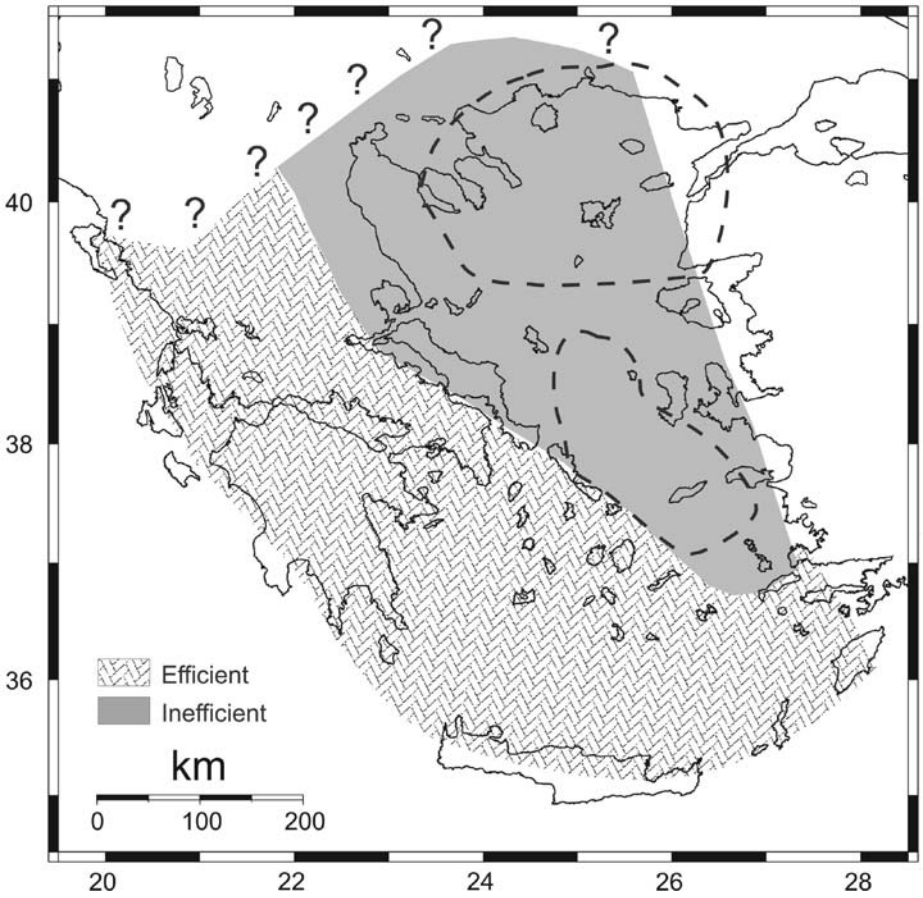

Figure 4. Geographical sketch that summarizes the observations of shear-wave propagation characteristics for the Aegean and surrounding areas. The dashed lines delineate the areas where low velocity bodies have been detected by previous studies in central/southeast Aegean (Karagianni *et al.*, 2005) and in northern Aegean (Bourova *et al.*, 2005).

The second group of inefficient ray paths traverses mostly the back-arc area of northern Aegean. In this case, we interpret the apparent shear-wave attenuation as the result of the ongoing extension of the back arc that is likely to cause elevated upper mantle temperatures (Currie and Hyndman, 2006). This suggestion is further supported by the following: (1) the high heat flow observed in the area (~2.5 HFU) (Jongsma, 1974), (2) observations of inefficient *Sn*-wave propagation in the northern Aegean (Gök *et al.*, 2000), and (3) the detection of a large, low-velocity anomaly (velocity contrast up to −4% compared with the IASPEI91 model for the area) between 70–100-km depth after surface-wave dispersion analysis (Bourova *et al.*, 2005). Even though limited resolution did not allow the determination of the exact shape of this area, Bourova *et al.* estimated that it should be at least 250-km wide, extending westwards from the Turkish coast to most of the northern Aegean, a suggestion that is also confirmed by our inefficient ray-path distribution.

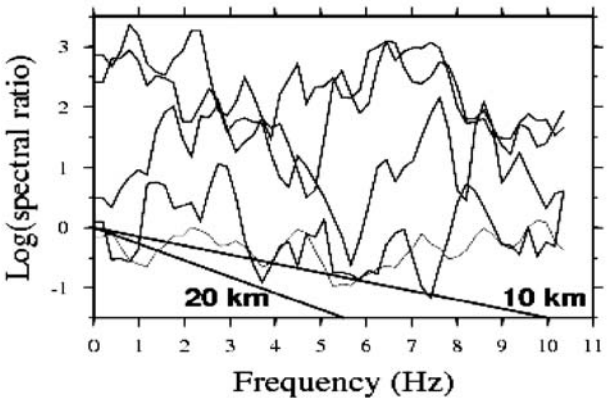

Figure 5. Diagram showing spectral ratios between pairs of earthquakes for different depth intervals (see text for details). Straight lines represent the spectral decay expected for paths along the slab that include a gap of 10 and 20 km, respectively.

Conclusions

The main conclusions of this study are as follows:

1. Shear waves generated by intermediate-depth earthquakes along the Hellenic arc are only slightly attenuated (average $Q_s \sim 1100$) when they propagate through the descending slab, and their ray paths cover most of the forearc area, providing additional constraints for the slab geometry.

2. The slab appears to be continuous downdip for the depth range between 60–160 km. However, if a gap along the dip does exist, it should be smaller than 10 km in order not to affect significantly the propagation of shear waves.
3. Two highly attenuating areas have been observed in the central/northern Aegean that correspond to the mantle wedge and the back-arc area, which is currently under extension. These areas also coincide with delineated low-velocity zones reported previously by other studies.

Acknowledgments

The present work was partly supported by North Atlantic Treaty Organization (NATO) Collaborative Linkage Grant Number 979849. The first author was also supported by the National Science Council of Taiwan. We would like to thank two anonymous reviewers and especially the associate editor, Keith Koper, whose comments and suggestions improved the original manuscript substantially.

References

Barazangi, M., and B. Isacks (1971). Lateral variations of seismic wave attenuation in the upper mantle above the inclined earthquake zone of the Tonga island arc: deep anomaly of the upper mantle, *J. Geophys. Res.* **76,** 8493–8516.

Barazangi, M., B. Isacks, and J. Oliver (1972). Propagation of seismic waves through and beneath the lithosphere that descends under the Tonga Island Arc, *J. Geophys. Res.* **77,** 952–958.

Barazangi, M., B. Isacks, J. Oliver, J. Dubois, and G. Pascal (1973). Descent of lithosphere beneath New Hebrides, Tonga-Fiji and New Zealand: evidence for detached slabs, *Nature* **242,** 98–101.

Benetatos, C., A. Kiratzi, C. Papazachos, and G. Karakaisis (2004). Focal mechanisms of shallow and intermediate depth earthquakes along the Hellenic arc, *J. Geodyn.* **37,** no. 2, 253–296, doi 10.1016/j.jog.2004.02.002.

Bourova, E., I. Kassaras, H. A. Pedersen, T. Yanovskaya, D. Hatzfeld, and A. Kiratzi (2005). Constraints on absolute S velocities beneath the Aegean Sea from surface wave analysis, *Geophys. J. Int.* **160,** no. 3, 1006–1019, doi 10.1111/j.1365-246X.2005.02565.x.

Currie, C. A., and R. D. Hyndman (2006). The thermal structure of subduction zone back arcs, *J. Geophys. Res.* **111,** B08404, doi 10.1029/2005JB004024.

Delibasis, N. D. (1982). Seismic wave attenuation in the upper mantle beneath the Aegean region, *Pure Appl. Geophys.* **120,** 820–839.

DeMets, C., R. G. Gordon, D. F. Argus, and S. Stein (1990). Current plate motions, *Geophys. J. Int.* **101,** 425–478.

Eberhart-Phillips, D., and M. Chadwick (2002). Three-dimensional attenuation model of the shallow Hikurangi subduction zone in the Raukumara Peninsula, New Zealand, *J. Geophys. Res.* **107,** no. B2, doi 10.1029/2000JB000046.

Galanopoulos, D., V. Sakkas, D. Kosmatos, and E. Lagios (2005). Geoelectric investigation of the Hellenic subduction zone using long period magnetotelluric data, *Tectonophysics* **409,** 73–84, doi 10.1016/j.tecto.2005.08.010.

Gök, R., N. Türkelli, E. Sandvol, D. Seber, and M. Barazangi (2000). Regional wave propagation in Turkey and surrounding regions, *Geophys. Res. Lett.* **27,** 429–432.

Hashida, T., G. Stavrakakis, and K. Shimazaki (1988). Three-dimensional seismic attenuation structure beneath the Aegean region and its tectonic implication, *Tectonophysics* **145,** 43–54.

Jongsma, D. (1974). Heat flow in the Aegean area, *Geophys. J. R. Astr. Soc.* **37,** 337–346.

Karagianni, E. E., C. B. Papazachos, D. G. Panagiotopoulos, P. Suhaldoc, A. Vuan, and G. F. Panza (2005). Shear velocity structure in the Aegean area obtained by inversion of Rayleigh waves, *Geophys. J. Int.* **160,** 127–143, doi 10.1111/j.1365-246X.2005.02354.x.

Klein, F. (2002). User's guide to Hypoinverse 2000, a FORTRAN program to solve for earthquake locations and magnitudes, *U.S. Geol. Surv. Open-File Rept. 02-171*.

Konstantinou, K. I., I. S. Kalogeras, N. S. Melis, M. C. Kourouzidis, and G. N. Stavrakakis (2006). The 8 January 2006 earthquake (Mw 6.7) offshore Kythira island, southern Greece: Seismological, strong-motion and macroseismic observations of an intermediate depth event, *Seism. Res. Lett.* **77,** 540–549.

Mele, G. (1998). High-frequency wave propagation from mantle earthquakes in the Tyrrhenian Sea: new constraints for the geometry of the south Tyrrhenian subduction zone, *Geophys. Res. Lett.* **25,** 2877–2880.

Melis, N. S., and K. I. Konstantinou (2006). Real-time seismic monitoring in the Greek region: an example of the 17 October 2005, East Aegean Sea earthquake sequence, *Seism. Res. Lett.* **77,** 364–370.

Oliver, J., and B. Isacks (1967). Deep earthquake zones, anomalous structure in the upper mantle and the lithosphere, *J. Geophys. Res.* **72,** 4259–4275.

Papazachos, C., and G. Nolet (1997). P and S deep velocity structure of the Hellenic area obtained by robust nonlinear inversion of travel times, *J. Geophys. Res.* **102,** 8349–8367.

Papazachos, B. C., V. G. Karakostas, C. B. Papazachos, and E. M. Scordilis (2000). The geometry of the Wadati-Benioff zone and lithospheric kinematics in the Hellenic arc, *Tectonophysics* **319,** 275–300.

Roth, E. G., D. A. Wiens, L. M. Dorman, J. Hildebrand, and S. C. Webb (1999). Seismic attenuation tomography of the Tonga-Fiji region using phase pair methods, *J. Geophys. Res.* **104,** 4795–4809.

Salah, K. M., and D. Zhao (2003). Three-dimensional attenuation structure beneath southwest Japan estimated from spectra of microearthquakes, *Phys. Earth Planet. Interiors* **136,** 215–231, doi 10.1016/S0031-9201(03)00049-9.

Schurr, B., G. Asch, A. Rietbrock, R. Trumbull, and C. Haberland (2003). Complex patterns of fluid and melt transport in the central Andean subduction zone revealed by attenuation tomography, *Earth Planet. Sci. Lett.* **215,** 105–119, doi 10.1016/S0012-821X(03)00441-2.

Spakman, W., M. J. R. Wortel, and N. J. Vlaar (1988). The Hellenic subduction zone: A tomographic image and its dynamic implications, *Geophys. Res. Lett.* **15,** 60–63.

Stachnik, J. C., G. A. Abers, and D. H. Christensen (2004). Seismic attenuation and mantle wedge temperatures in the Alaska subduction zone, *J. Geophys. Res.* **109,** B10304, doi 10.1029/2004JB003018.

Tsokas, G. N., and R. O. Hansen (1997). Study of the crustal thickness and the subducting lithosphere in Greece from gravity data, *J. Geophys. Res.* **102,** 20,585–20,597.

Tsumura, N., S. Matsumoto, S. Horiuchi, and A. Hasegawa (2000). Three-dimensional attenuation structure beneath the northeastern Japan arc estimated from spectra of small earthquakes, *Tectonophysics* **319,** 241–260.

Umino, N., and A. Hasegawa (1984). Three-dimensional Q_s structure in the northeastern Japan arc, *J. Seism. Soc. Jpn.* **37,** 217–228.

Institute of Geophysics
National Central University
No. 300 Jhongda Road
Jhongli, 320 Taiwan
kkonst@ncu.edu.tw
(K.I.K.)

Institute of Geodynamics
National Observatory of Athens
P.O. Box 20048
GR-11810, Athens, Greece
(N.S.M.)

Manuscript received 14 November 2006